Hindawi
Mathematical Problems in Engineering
Volume 2022, Article ID 7949419, 13 pages
https://doi.org/10.1155/2022/7949419

Research Article

Wind-Thermal-Energy Storage System Optimization: Evidence from Simulations of the Economical Consumption of Wind Energy

Shouwen Wang,[1] **Jiejia Zhang**,[2] **and Zhaobin Zhu**[2]

[1]*School of Law and Public Administration, China Three Gorges University, Yichang 443002, China*
[2]*College of Electrical and New Energy, China Three Gorges University, Yichang 443002, China*

Correspondence should be addressed to Zhaobin Zhu; 202008080021051@ctgu.edu.cn

Received 6 August 2022; Revised 1 October 2022; Accepted 3 October 2022; Published 7 November 2022

Academic Editor: Yang Li

To realize the economical consumption of wind energy (WE), an optimal dispatch strategy for wind-thermal-energy storage systems (WTESSs) is proposed. The scheduling model is divided into two stages. In the first stage, the strategy aims to shave peaks and fill valleys in the load curve using a time-of-use (TOU) electricity price and to reduce the variance of the net load and use the energy time-shift characteristics of energy storage systems (ESSs) to optimize their charging and discharging power. In the second stage, the strategy minimizes the cost of WTESSs, obtaining the output power of the thermal power units (TPUs) in each period. Considering the actual need for carbon reduction, a method for calculating the TPUs' life loss cost under different variable load amplitudes is introduced, and a thermal power peaking cost model considering the ladder-type carbon trading model is constructed to calculate the cost accurately. In addition, to account for the fact that connecting all wind power outputs to the grid will significantly increase the grid peak regulation pressure and operational risk, a mathematical model for WE utilization is established to find the optimal power value for wind power grid connection in each period, which enables economical and practical WE scheduling. According to the simulation results, the overall peak-shaving cost of the system can be reduced by up to 23.95%, and the thermal power deep peak regulation cost can be reduced by up to 90.06%.

1. Introduction

With the exacerbation of energy scarcity and the greenhouse effect, action to reduce pollution and carbon emissions is urgently needed [1]. A global consensus has been reached to accelerate the transition to green energy and sustainable development [2]. According to the Global Wind Energy Report 2022 from the Global Wind Energy Council, a 557 GW increase in global wind power is expected over the period 2022–2026, with a compound annual growth rate of 6.6% [3]. With the rapid development of the sector, wind energy (WE) has emerged as a key energy source on a global scale [4]. Realizing the low-carbon economic potential of WE is a current research focus [5, 6].

WE grid connection should be planned in view of comprehensive social costs, such as the corresponding peaking cost and carbon emission cost [7, 8]. Many countries use WE wisely: generally, the United States and certain European nations do not use all of their available WE [9]. For example, the rate of WE curtailment is approximately 5% in the United Kingdom and Ireland [10]. In some parts of Germany, wind power generators and electricity distribution companies accept reasonable levels of WE curtailment under transparent conditions, such as including wind curtailment clauses in grid-connection agreements or power-purchase contracts and allowing 1%–5% of wind power to be curtailed [11, 12]. These countries support a green and low-carbon transformation of the energy structure at the lowest possible cost and do not see the full grid-integrated accommodation of WE consumption as a development goal.

Numerous studies have shown that the outputs of WE generators are random, erratic, and have evident antipeak-

shaving characteristics [13, 14]. If WE is fully incorporated into the power system indiscriminately, the safety, stability, and economics of grid operation will encounter significant obstacles [15]. According to statistics from the China State Grid Energy Research Institute, a "low peak power ratio" is a hallmark of many Chinese provinces' WE power-generating outputs. Not using a portion of the peak power can considerably lower the system pressure without greatly impairing the annual output of new energy sources [16]. Therefore, appropriately curtailing a certain amount of wind power under certain conditions, that is, when WE is abundant and the load demand is low, can improve the flexibility of power grid dispatch, which is an important measure of the economical consumption of WE [17, 18].

Bird et al. [19] made a review of international experience in the curtailment of wind and solar energy on bulk power systems in recent years, in which it is shown that curtailment can help mitigate excess generation and provide ancillary services. Xu et al. [20] adopted the safety-constrained economic dispatch model, introduced a sectional penalty factor for wind power curtailment, prioritized wind power consumption, and curtailed wind from each wind farm in a rational manner according to a preestablished wind power curtailment principle. Wang et al. [21] conducted a large-scale analysis of the history of wind power output and presented a theoretical research method for the rational use of high-power wind output under low loads. Y. B. Wang [22] explored the problem of the rational curtailment of new energy and found a balance between the cost and benefit of new energy consumption. Using the GESP power planning software, the study took China's major regional power grids as an example and calculated a rational energy curtailment rate of 3%–10% for 2020. Golden and Paulos [23] provided a detailed explanation of the potential positive and negative impacts of curtailment, proposing a policy that can be used to blaze a trail to a low-carbon future through greater use of renewable electricity in California.

Thermal power units (TPUs) still make up a large percentage of the energy structure in northern China [24]. Although large-scale wind power integration can minimize CO_2 emissions, it can also push TPUs away from their ideal economic operating point [25]. Demand response (DR) dispatching enables a high level of flexibility according to studies in several countries. DR dispatching can be used to explore potential interactions between various user loads [26], and it also diminishes the load peak-to-valley difference [27], which effectively enhances load-side adaptability. A review of the literature reveals the importance of DR dispatching in promoting the accommodation of new energy [28]. DR dispatching can also be used as an incentive mechanism on the user side to promote the rational allocation of resources on the source and load sides [29].

Additionally, energy storage systems (ESSs) have an essential regulatory impact on the source, grid, and load sides [30] due to their effective charging and discharging characteristics, which enable rapid power regulation [31]. Therefore, the combined use of DR dispatching and ESSs as peak-shaving resources in power system scheduling is often considered, as it can effectively enhance the economic benefits of TP operation and stabilize the power system.

The use of ESSs and DR dispatching for multisource joint optimal scheduling is an effective measure to alleviate the difficulty of peak regulation for new energy-connected grids. Hamidpour et al. [32] made disruptive changes to the existing power system structures and procedures of wind farms and ESSs and took into account demand-side flexibility requirements. Hosseini Imani et al. [33] analyzed the effect of running the TOU response program and used ESS units to compensate for the stochastic nature of WE generation. MohammadGholiha et al. [34] used DR dispatching and an ESS to alleviate the uncertainties in wind power and electrical load and formulated a two-stage stochastic programming model for optimal reserve determination. In reference [35], novel DR applications were modeled to quantify additional reductions in the curtailed WE, and various combinations of ESS and DR dispatching were considered to investigate their impacts on further reducing wind curtailment. Jamali et al. [36] used ESSs and DR dispatching and proposed a stochastic bidding strategy based on virtual power plants to increase the profit of virtual power plants in short-term electricity markets.

Building on the multiobjective optimization and comprehensive decision-making two-stage model proposed in [37], combined with the day-ahead energy trading two-stage model proposed in [38], this study establishes a two-stage optimal scheduling model. The model emphasizes the effective utilization of two peak-shaving resources: DR dispatching and ESSs. The first-stage model takes as input the adjusted load curve after accounting for the time-of-use (TOU) electricity price, and the optimal wind power-connected grid is obtained on this foundation by combining it with an ESS. The main function of the ESS is minimizing changes in the grid's net load. The optimal output power of the TPU is obtained in the second stage of the decision, and the wind-thermal-energy storage systems (WTESSs) cost is minimized. By comparing the simulated operations under various conditions, the viability and efficacy of this technique are proven, and the low-carbon economic regulation of wind power is achieved.

This study makes two main contributions:

(1) Theoretical contribution: This study dispenses with the traditional assumption of full grid connection of wind power, focusing on the consumption of total wind power rather than that of the grid-connected WE at any single moment. A model of the WE utilization rate at each time point is constructed, and the impact of the rational dispatch of wind power on the overall economic benefit of the power system is explored. This enables the active deployment of flexible resources in the power system, the design of a two-stage optimum scheduling model for WTESSs in the setting of a low-carbon economy, and the definition of a TPU deep peak regulation (DPR) cost function.

(2) Practical contribution: A workable methodology for dispatching WE is advanced that combines power

grid safety, cost-effectiveness, and environmental preservation. This methodology is beneficial for WE scheduling by bringing the dispatching of power system security into consideration, thus bolstering the health and long-term growth of the WE market.

2. Methodology

2.1. DR Model Based on TOU

2.1.1. Load Change Rate considering Load Characteristic Classification. User loads can vary depending on the price signal and can be simply classified as reduced loads and transfer loads. Taking into account load characteristics, the users' peak period power consumption following the application of the TOU electricity price can be stated by the following two sets of equations:

$$Q_f^1 = Q_f^0 - \Delta Q_f = Q_f^0 - \left(\Delta Q_f^{\text{red}} + \Delta Q_f^{\text{trans}}\right), \cdot \begin{cases} \Delta Q_f^{\text{red}} = \phi_f^{red} \times Q_f^0, \\ \Delta Q_f^{\text{trans}} = \Delta Q_{fp}^{\text{trans}} + \Delta Q_{fg}^{\text{trans}} = \phi_{fp}^{\text{trans}} \times Q_f^0 + \phi_{fg}^{\text{trans}} \times Q_f^0 \end{cases}, \tag{1}$$

where $Q1/f$ and $Q0/f$ denote the loads during the peak period before and after the TOU, respectively; ΔQ_f represents the load variation after the TOU; $\Delta Q\text{red}/f$ and $\Delta Q\text{trans}/f$ represent the load reduction and load transformation during the peak period after TOU, respectively; $\phi\text{red}/f$ is the load reduction rate at the peak period; $\Delta Q\text{trans}/fp$ and $\phi\text{trans}/fp$ are the load transfer quantity and rate from the peak period to the flat period, respectively; $\Delta Q\text{trans}/fg$ and $\phi\text{trans}/fg$ denote the load transfer quantity and rate from the peak period to the valley period, respectively.

$$Q_t^1 = Q_t^0\left(1 + \varepsilon_{tt}\frac{\Delta D_t}{D_t^0} + \sum_{r=1, r\neq t}^{T} Q_t^0 \varepsilon_{tr}\frac{\Delta D_r}{D_r^0}\right), \cdot \begin{cases} \varepsilon_{tt} = \dfrac{\Delta Q_t/Q_t^0}{\Delta D_t/D_t^0}, \\ \varepsilon_{tr} = \dfrac{\Delta Q_t/Q_t^0}{\Delta D_r/D_r^0}, \end{cases} \tag{2}$$

where $Q0/t$ and $Q1/t$ are the electricity quantities in period t after the TOU, respectively; ε_{tt} and ε_{tr} are the self-elasticity and cross-elasticity, respectively (a rise in electricity prices will result in a drop in electricity during this period and an increase during other periods, so usually $\varepsilon_{tt} < 0$ and $\varepsilon_{tr} > 0$); ΔQ_t and ΔD_t are the change in electricity quantity and price in period t before and after the TOU, respectively; ΔD_r is the change in electricity price in period r before and after the TOU; T is the scheduling period, which is 24 h; $D0/t$ is the electricity price in period t before the TOU; $D0/r$ is the electricity price in period r before the TOU.

Let ϕ_t denote the change in the load rate in period t after the TOU; then,

$$\phi_t = \phi_t^{\text{red}} + \phi_t^{\text{trans}} = \varepsilon_{tt}\frac{\Delta D_t}{D_t^0} + \sum_{r=1}^{T} \varepsilon_{tr}\frac{\Delta D_r}{D_r^0}, \tag{3}$$

where $\phi\text{red}/t$ and $\phi\text{trans}/t$ are the load reduction rate and transfer rate in period t, respectively.

2.1.2. Load Response Model. Load reduction and load transfer rates are employed to appropriately represent the users' reaction to the TOU and the load characteristics of the peak, flat, and valley periods. The price of power during the flat period is denoted by $Qt/0$, and the peak-to-flat and valley-to-flat electricity price floating ratios are written as follows:

$$\begin{cases} K_f = \dfrac{\left(D_f - D_p\right)}{D_p}, \\ K_g = \dfrac{\left(D_g - D_p\right)}{D_p}, \end{cases} \tag{4}$$

where K_f represents the fluctuating ratio of the electricity price from the peak period to the flat period; K_g represents the fluctuating ratio of the electricity price from the valley period to the flat period; D_f, D_p, and D_g represent the electricity prices during the peak, flat, and valley periods, respectively.

The load reduction rate and transfer rate of the users at any time are represented as follows when the definitions of (2) and (3) are combined.

$$\begin{cases} \phi_{ff} = K_f \varepsilon_{tt} \; \forall t \in T_f, \\ \phi_{pp} = 0 \; \forall t \in T_p, \\ \phi_{gg} = K_g \varepsilon_{tt} \; \forall t \in T_g, \\ \phi_{fp} = K_f \varepsilon_{tr} \; \forall t \in T_f, \; \forall r \in T_p, \\ \phi_{fg} = \left(K_f - K_g\right)\varepsilon_{tr} \; \forall t \in T_f, \; \forall r \in T_g, \\ \phi_{pg} = -K_g \varepsilon_{tr} \; \forall t \in T_p, \; \forall r \in T_g, \end{cases} \tag{5}$$

where ϕ_{ff}, ϕ_{pp}, and ϕ_{gg} are the load decrease rates during the peak, flat, and valley periods, respectively (because $K_f > 0, K_p = 0, K_g < 0$, we usually have $\phi_{ff} < 0, \phi_{pp} < 0$, $\phi_{gg} < 0$); ϕ_{fp}, ϕ_{fg}, and ϕ_{pg} are the load transfer rates during the peak-to-flat, peak-to-valley, and flat-to-valley periods, respectively.

Finally, the load response model that takes into account the mechanism of action of the TOU is as follows:

$$\begin{cases} Q_{f,t}^1 = Q_{f,t}^0 + \phi_{ff} Q_{f,t}^0 - \phi_{fp} Q_{f,t}^0 - \phi_{fg} Q_{f,t}^0 \forall t \in T_f, \\ Q_{p,t}^1 = Q_{p,t}^0 + \phi_{fp} Q_{f,t}^0 + \phi_{pp} Q_{p,t}^0 - \phi_{pg} Q_{p,t}^0 \forall t \in T_p, \\ Q_{g,t}^1 = Q_{g,t}^0 + \phi_{fg} Q_{f,t}^0 + \phi_{pg} Q_{p,t}^0 + \phi_{gg} Q_{g,t}^0 \forall t \in T_g. \end{cases} \tag{6}$$

2.2. Peak-Shaving Model for TPU considering LCT

2.2.1. DPR Process of TPU. $P_{\max}$ is the TPU's maximum output; $P_{\min}$ is its minimum output under regular peak

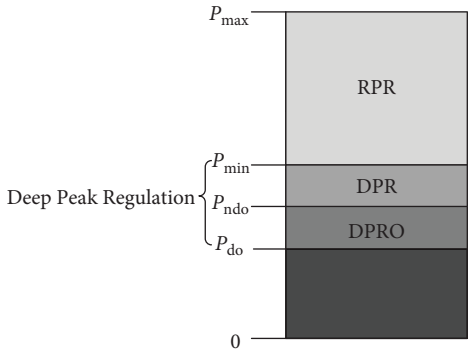

Figure 1: Schematic diagram of TPU operates in RPR, DPR, and DPRO.

regulation (RPR); P_{ndo} is its minimum output under DPR; P_{do} is its minimum output under deep peak regulation with oil (DPRO), as shown in Figure 1.

2.2.2. LCT Model. To control carbon emissions, a carbon trading scheme is established. Each carbon emission source has a certain amount of carbon emission allowances, according to which producers arrange their production. If producers emit less carbon than the corresponding allowances, the remaining allowances can be sold through the carbon trading market, whereas if they exceed the corresponding allowances, additional allowances must be purchased. To solve the problems of the traditional carbon trading pricing mechanism, which has only a weak effect on carbon emissions, the LCT pricing mechanism is adopted, in which the carbon emission price varies with the distribution of additional carbon emission rights that producers need to purchase.

(1) Initial Carbon Emission Quota

$$E_{\text{free}} = \psi_{\text{free}} \sum_{t=1}^{T} \sum_{i=1}^{N_G} P_{i,t}^{\text{unit}}, \tag{7}$$

where E_{free} is the TPUs' total allowance for carbon emissions; ψ_{free} is the allowable amount of carbon emissions per unit of energy used; N_G is the total number of TPUs; $P\text{unit}/i,t$ is the output value of TPUs in period t.

(2) Actual Carbon Emissions

$$E_{CO_2} = \sum_{t=1}^{T} \sum_{i=1}^{N_G} \beta_{2i} \left(P_{i,t}^{\text{unit}}\right)^2 + \beta_{1i} P_{i,t}^{\text{unit}} + \beta_{0i}, \tag{8}$$

where E_{CO_2} are the total real carbon emissions from all TPUs; β_{2i}, β_{1i}, and β_{0i} are the variables used to calculate each TPU's carbon emissions.

(3) Carbon Trading Cost

$$C_{CO_2} = \begin{cases} -b(1+2\delta)\left(E_{\text{free}} - l - E_{CO_2}\right) & E_{CO_2} \le E_{\text{free}} - l \\ -b(1+2\delta)l - b(1+\delta)\left(E_{free} - E_{CO_2}\right), & E_{free} - l < E_{CO_2} \le E_{\text{free}} \\ b\left(E_{CO_2} - E_{\text{free}}\right) & E_{free} < E_{CO_2} \le E_{\text{free}} + l \\ bl + b(1+\delta)\left(E_{CO_2} - E_{\text{free}} - l\right) & E_{\text{free}} + l < E_{CO_2} \le E_{\text{free}} + 2l \\ (2+\delta)l + b(1+2\delta)\left(E_{CO_2} - E_{\text{free}} - 2l\right), & bE_c + 2l < E_{CO_2} \le E_{\text{free}} + 3l \\ b(3+3\delta)l + b(1+3\delta)\left(E_{CO_2} - E_{\text{free}} - 3l\right), & E_{CO_2} > E_{\text{free}} + 4l \end{cases}, \tag{9}$$

where C_{CO_2} denotes the carbon trading cost; b denotes the carbon trading base price; δ denotes the price growth rate; l denotes the carbon emission range.

2.3. DPR Cost Model for TPUs considering LCT

(1) Under usual circumstances, the TPU operates in the RPR. During that time, C_{coal} represents the peak-shaving cost. TPUs generate significant carbon emissions. The peak-shaving cost of C_{unit1}, taking LCT into account, is calculated as follows:

$$\begin{aligned} C_{unit1} &= C_{coal} + C_{CO_2}, \\ C_{coal} &= \sum_{t=1}^{T} \sum_{i=1}^{N_G} \alpha_{2i} \left(P_{i,t}^{unit}\right)^2 + \alpha_{1i} P_{i,t}^{unit} + \alpha_{0i}. \end{aligned} \tag{10}$$

Here, α_{2i}, α_{1i}, and α_{0i} are the coal consumption cost coefficients associated with TPU i.

(2) The TPUs must lower their output and transition into the DPR stage when additional energy is incorporated into the grid on a considerable scale, especially during the low load time at night. When a TPU's output is between $P_{\min}$ and the P_{ndo}, the rotor metal experiences alternating stress that causes low-cycle fatigue loss, which raises the TPU loss cost C_{unit2}:

$$C_{\text{unit2}} = \delta_i^{\text{unit}} S_{\text{unit-price}}. \tag{11}$$

Here, $\delta(\text{unit}/i)$ is the life loss rate of the TPU.

(3) More fuel will be required to keep the boiler burning steady if the grid-integrated capacity of new energy sources grows while the TPU is running at a low

load. As a result, the TPU incurs increased oil costs, entering DPRO. The following equation is derived.

$$C_{\text{unit3}} = Q_{\text{oil}} S_{\text{oil-price}}, \tag{12}$$

where $S_{\text{oil-price}}$ is the oil price; Q_{oil} is the oil consumption in DPRO.

To summarize, the following is an expression for the peak-shaving cost of TPUs:

$$C_{\text{unit}} = \begin{cases} C_{\text{unit1}}, & P_{\min} < P \le P_{\max}, \\ C_{\text{unit1}} + C_{\text{unit2}}, & P_{ndo} < P \le P_{\min}, \\ C_{\text{unit1}} + C_{\text{unit2}} + C_{\text{unit3}}, & P_{do} \le P \le P_{ndo}. \end{cases} \tag{13}$$

Given that C_{unit} is a discontinuous function, (11) is transformed into a continuous function in the form of linear constraints using Boolean variables:

$$\begin{aligned} C_{\text{unit}} &= C_{\text{unit1}} + X_{bty} C_{\text{unit2}} + Y_{ty} C_{\text{unit3}}, \\ X_{bty} &= \begin{cases} 0, & P_{\min} < P \le P_{\max}, \\ 1, & P_{ndo} < P \le P_{\min}, \end{cases} \\ Y_{ty} &= \begin{cases} 0, & P_{ndo} < P \le P_{\min}, \\ 1, & P_{do} \le P \le P_{ndo}, \end{cases} \end{aligned} \tag{14}$$

where X_{bty} and Y_{ty} are the Boolean variables corresponding to the life loss cost and the oil cost, respectively.

2.4. Two-Stage Optimal Scheduling Model. Having established the above basic model, a two-stage optimal scheduling model of the WESS is constructed; its structure is shown in Figure 2. The open-source solver CPLEX [39], developed by IBM, is used to represent complex economic problems as mathematical programming models. It is based on a fusion of the branch-cut plane method, interior point method, and other methods such as preprocessing and heuristics to enable rapid solutions to these problems. The scheduling model in this study is a mixed integer quadratic model designed to transform the practical problem of economical wind power dispatch into a mathematical model for solving the utilization rate of each time period, for which CPLEX is highly suitable.

2.4.1. First-Stage Model

(1) Objective Function. In the first stage, with consideration of the TOU and ESS, the grid-connected wind power and the ESS's charge–discharge power is optimized with the aim of reducing the variance in the net load, while satisfying the corresponding restrictions. The following objective function intends to enhance the valley load and cut peak load, lessen the net load fluctuation, and avoid frequent output adjustments for TPUs.

$$\min A = \frac{1}{T} \sum_{t=1}^{T} \left(L_{net,t} - L_{net,ave} \right)^2,$$

$$\begin{cases} L_{\text{net,t}} = Q_t^1 - \lambda_{w,t}^{\text{use}} P_{w,t}^{tot} + \eta_{es}^{cha} P_{es,t}^{cha} - \eta_{es}^{dis} P_{es,t}^{dis}, \\ L_{\text{net,ave}} = \dfrac{\sum_{t=1}^{T} L_{net,t}}{T}, \end{cases} \tag{15}$$

where A is the variance in the grid's net load; $L_{net,t}$ is the net load value in period t; $L_{net,ave}$ is the average value of the net load during the whole dispatch period; $Q1/t$ is the load value after the TOU; $\lambda use/w,t$ is the rate at which WE is used in period $t\,(0 \le \lambda use/w, t \le 1)$; $Ptot/w,t$ represents the wind farm's output power value; $Pcha/es,t$ and $Pdis/es,t$ represent the charging and discharging power values, respectively; $\eta cha/es$ and $\eta dis/es$ indicate the charge and discharge efficiencies of the ESS, respectively.

(2) Constraints

(1) Wind power output constraints

The grid-connected wind power in each period is less than the actual output power of the wind farm

$$0 \le P_{w,t}^{tot} \le P_{w,t}^{\max}. \tag{16}$$

Here, $P\max/w,t$ indicates the greatest output of the wind farm during period t.

(2) WE utilization constraints

To avoid a large amount of wind curtailment due to the minimization of the net load variance under the optimized solution, a minimum utilization rate of WE is stipulated

$$\frac{\sum_{t=1}^{T} \lambda_{w,t}^{\text{use}} P_{w,t}^{tot}}{\sum_{t=1}^{T} P_{w,t}^{tot}} \ge R_{w,\min}. \tag{17}$$

Here, $R_{w,\min}$ is the minimal total WE utilization.

(3) Charge and discharge power constraints

$$\begin{aligned} 0 \le P_{es,t}^{cha} \le P_{es,\max}^{cha}, \\ 0 \le P_{es,t}^{dis} \le P_{es,\max}^{dis}. \end{aligned} \tag{18}$$

Here, $P_{es,t}^{cha}$ and $P_{es,\max}^{dis}$ denote the maximum charge and discharge powers of the ESS, respectively.

(4) Charge and discharge logic state constraints

$$\begin{aligned} I_{es,t}^{cha} + I_{es,t}^{dis} \le 1, \\ \left(W_{es,t} + W_{es,t-1} \right) - I_{es,t}^{cha} + I_{es,t}^{dis} = 0. \end{aligned} \tag{19}$$

Here, $Icha/es,t$ and $Idis/es,t$ are binary variables used to transition between the charging state and the discharging state of the ESS, respectively (the ESS enters the charging state in period t when $Icha/es,t = 1$, signaling that it is going to be charged; the ESS switches from the charging state to the discharging state in period t when $Idis/es,t = 1$, indicating that it is going to be discharged). $W_{es,t}$ and $W_{es,t-1}$ represent the charging and discharging states of the ESS in period t and period t−1, respectively. (When the value is 1, the ESS is charging, and when the value is 0, the ESS is discharging.)

(5) State-of-charge (SOC) constraints

To ensure the sustainability of the ESS participating in the scheduling operation, SOC constraints need to be added.

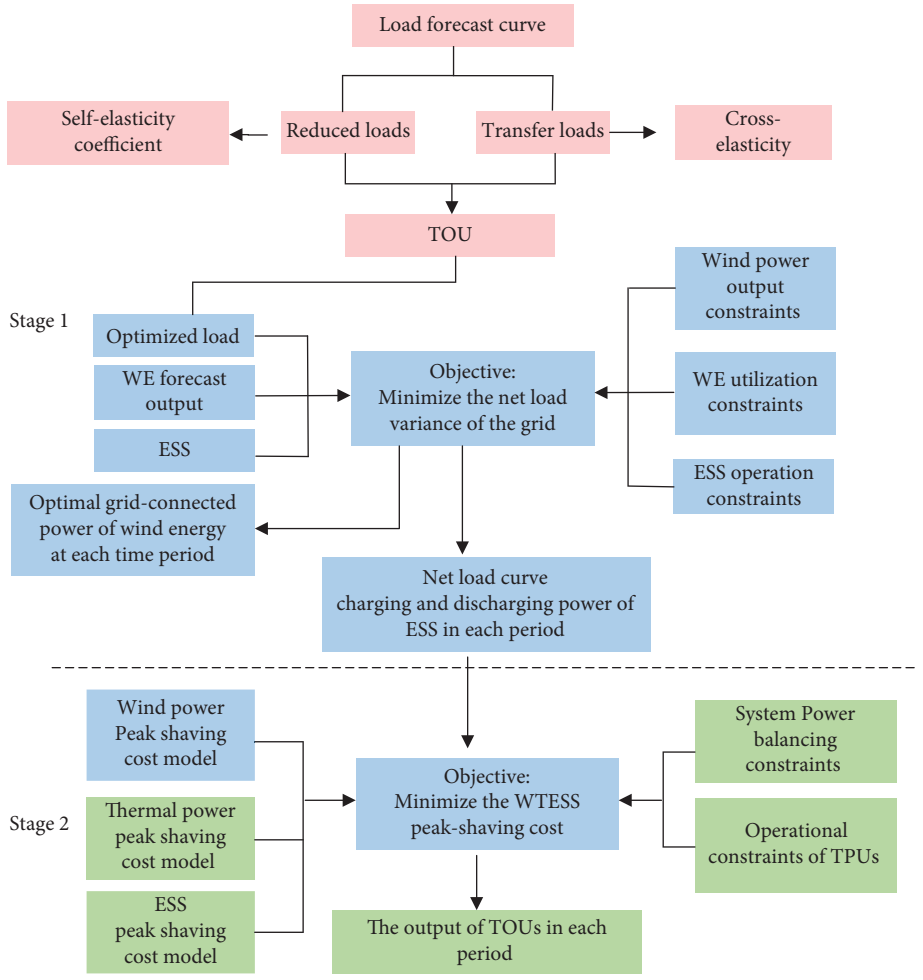

Figure 2: The schematic diagram of the two-stage optimal scheduling model.

$$S_{oc,\min} \le S_{oc,t} \le S_{oc,\max},$$

$$S_{oc} = S_{oc,t-1} + \frac{W_{es,t}\Delta T \eta_{es}^{cha} P_{es,t}^{cha}}{C_{es}^{cap}} - \frac{\left(1 - W_{es,t}\right)\Delta T P_{es,t}^{dis}}{\eta_{es}^{dis} C_{es}^{cap}}, \tag{20}$$

where $S_{oc,t}$ is the SOC for the ESS in period t; $S_{oc,\max}$ is the maximum SOC; $S_{oc,\min}$ is the minimum SOC; Ccap/*es* is the ESS's capacity.

2.4.2. Second-Stage Model

(1) Objective Function. The second stage determines the optimal outputs of the TPUs by satisfying various operation constraints, together with the net load curve that is inherited from the first stage. Minimizing the peak cost of the WESS is the objective of the second-stage model, and the solution indicates how economical the power system is. The objective solution accounts for the costs of wind power operation and maintenance, wind power curtailment, peak-shaving of thermal power plants, and peak-shaving of the ESS. The following is the formula:

$$\min B = C_{wyw} + C_{wqf} + C_{unit} + C_{es1} + C_{es2} + C_{es3}. \tag{21}$$

(1) Wind power operation and maintenance costs

$$C_{wyw} = \alpha_{wyw} P_{w,t}. \tag{22}$$

Here, α_{wyw} is the wind power operation coefficient.

(2) Wind curtailment penalty

$$C_{wqf} = \alpha_{wqf}\left(P_{w,t}^{tot} - P_{w,t}\right). \tag{23}$$

Here, α_{wqf} is the wind curtailment penalty coefficient.

(3) Charging and discharging cost of the ESS

$$C_{es1} = \sum_{t=1}^{T}\left(P_{es,t}^{cha} + P_{es,t}^{dis}\right)S_{\text{power-price}}. \tag{24}$$

Here, $S_{\text{power-price}}$ represents the charge and discharge cost per unit power of the ESS.

(4) Life loss cost of the ESS

$$C_{es2} = \frac{S_{\text{build-price}}}{O_{\text{cir}}} \sum_{t=1}^{T}\left(\frac{I_{es,t}^{cha} + I_{es,t}^{dis}}{2}\right). \tag{25}$$

Here, $S_{\text{build-price}}$ is the ESS's construction cost; O_{cir} is the ESS's cycle life.

(5) Additional environmental costs of the ESS

$$C_{es3} = \sum_{t=1}^{T} \eta_{es}^{dis} P_{es,t}^{dis} \mu_{\text{poll}} S_{\text{poll-price}}, \tag{26}$$

where μ_{poll} is the emission density of ESS-emitted pollutants; $S_{\text{poll-price}}$ is the unit emission cost of pollutants (the pollutants referred to in this paper are SO_2 and NO_x).

(2) Constraints

(1) Constraints on the system's power balance

When excluding the system network loss, the real-time load is equal to the total output power of TPUs and WE and the charge and discharge power of the ESS

$$\sum_{i=1}^{N_G} P_{i,t}^{\text{unit}} + \lambda_{w,t}^{\text{use}} P_{w,t}^{tot} + P_{es,t} = Q_t^1. \tag{27}$$

(2) TPU output constraints

$$P_{i,\min}^{\text{unit}} \le P_{i,t}^{\text{unit}} \le P_{i,\max}^{\text{unit}}. \tag{28}$$

Here, $P\text{unit}/i,\max$ is the maximum output of TPU i; $P\text{unit}/i,\min$ is the minimum output of TPU i.

(3) TPU climbing constraints

$$\begin{cases} P_{i,t}^{\text{unit}} - P_{i,t-1}^{\text{unit}} \le \Delta P_{i,up}^{\text{unit}}, \\ P_{i,t-1}^{\text{unit}} - P_{i,t}^{\text{unit}} \le \Delta P_{\text{i,down}}^{\text{unit}}. \end{cases} \tag{29}$$

Here, $\Delta P\text{unit}/i,up$ denotes the TPU's capacity to ascend to its upper limit, and $\Delta P\text{unit/i, down}$ denotes its ability to drop to its lower limit.

(4) Line transmission capacity constraints

$$0 \le P_{\text{line,t}} \le P_{\text{line,t}}^{\max}, \tag{30}$$

Where $P_{\text{line,t}}$ is the line's transmission power in period t; $P\text{max/line, t}$ is the line's maximum transmission capacity in period t.

3. Results and Discussion

3.1. Simulation Parameters. Specific parameters for the TPUs are shown in Table 1. The load characteristic data are referenced from Ref. [45]; the wind power forecast data are referenced from Ref. [46], and Figure 3 depicts the categorized user load curve and wind power output curve.

Other relevant parameters are as follows:

(1) Because there are significant differences in the degree to which various users participate in the TOU, the elasticity coefficient, and the division of peak, flat, and valley periods, this study classifies users into industrial, commercial, and residential users. Table 2 itemizes the peak, flat, Table 3 and valley periods for the three different user groups as well as the peak-to-valley price variations in relation to the initial price of power and the corresponding price elasticity coefficients. (The electricity price is expressed in CNY/kWh and remains constant during the flat period, rises during the peak period, and falls during the valley period.) Additionally, it is assumed that 20% of commercial and residential users and 50% of industrial users engage in the TOU.

(2) The minimum output values of coal-fired power units in RPR, DPR, and DPRO are 50%, 40%, and 30% of the unit capacity, respectively. The rotor boiler is a typical material of 30Cr2MoV steel and displays the life loss rate of a coal-fired power unit under various load fluctuations.

(3) The cost of the unit capacity of a coal-fired power unit is 3,464,000 CNY/MW; the unit price of coal is 500 CNY/t; the carbon emission allowance per unit power consumption of TPUs is 759.8 kg/(MWh); the base price of carbon trading is 250 CNY/t; the price growth rate is 25%; the fuel consumption of TPUs in DPRO is 4.8 t/h; and the unit price of oil is 6,130 CNY/t.

(4) ESS parameters: the capacity is 400 MW, the initial state of charge is 0.1, the upper limit of the SOC is 0.9, and the lower limit of the SOC is 0.1; the charge and discharge efficiency are both 0.9.

(5) Parameters of the additional environmental cost of the ESS: the emission densities of SO_2 and NO_x are 1.8 kg/(MWh) and 1.6 kg/(MWh), respectively, and their unit emission costs are 14.842 CNY/kg and 62.964 CNY/kg, respectively. Through conversion, the pollutant emission price corresponding to each MWh of electricity is 127.5 CNY.

3.2. Results

3.2.1. TOU Optimization Results. The load curves before and after the TOU for industrial, commercial, and residential users can be seen in Figure 4. Industrial customers have more flexibility and adaptability in power consumption, so the peak-shaving and valley-filling impacts are more visible for these customers. Commercial and residential customers have more fixed power consumption times and a lower proportion of users that respond to the changes. Therefore, the influence of TOU on peak-shaving and valley-filling is not as large as that of industrial users.

3.2.2. Analysis of Optimization Results. The total load curve prior to and following TOU, the net load curve prior to and following the first stage of model optimization, the wind power integrated into the power grid curve, and the WE utilization rate throughout all periods can be seen in Figure 5. The peak-to-valley difference of the entire load curve is 965.1 MW, which is 251.65 MW less than that before the TOU. This difference permits additional space for wind power grid connection. The graph illustrates that wind curtailment does not occur except at 1 : 00, 2 : 00, 4 : 00, and 24 : 00, and the wind energy consumption rate is 100% at all other times. By combining the wind power output curve and the load characteristic curve, it can be observed that wind curtailment is maximized at times of low load and large wind

Table 1: Parameters of the thermal power unit.

Capacity of thermal power unit	Fuel cost factor			Climb slope rate (MW/h)	Carbon cost factor		
	α_{2i} (CNY)	α_{1i} (CNY/MW)	α_{0i} (CNY/MW2)		β_{2i} (t)	β_{1i} (t/MW)	β_{0i} (t/MW2)
600 MW	0.006	98.607	4093.557	300	29.04	0.68	0.00016
300 MW	0.047	82.936	5716.897	150	15.8	0.788	0.0000937
300 MW	0.047	82.936	5716.897	150	15.8	0.788	0.0000937
200 MW	0.401	102.607	1454.864	100	10.81	0.863	0.000121
100 MW	1.156	115.640	2327.998	50	3.82	0.9	0.000246
50 MW	4.130	66.080	2091.432	25	0.75	0.9121	0.0002814

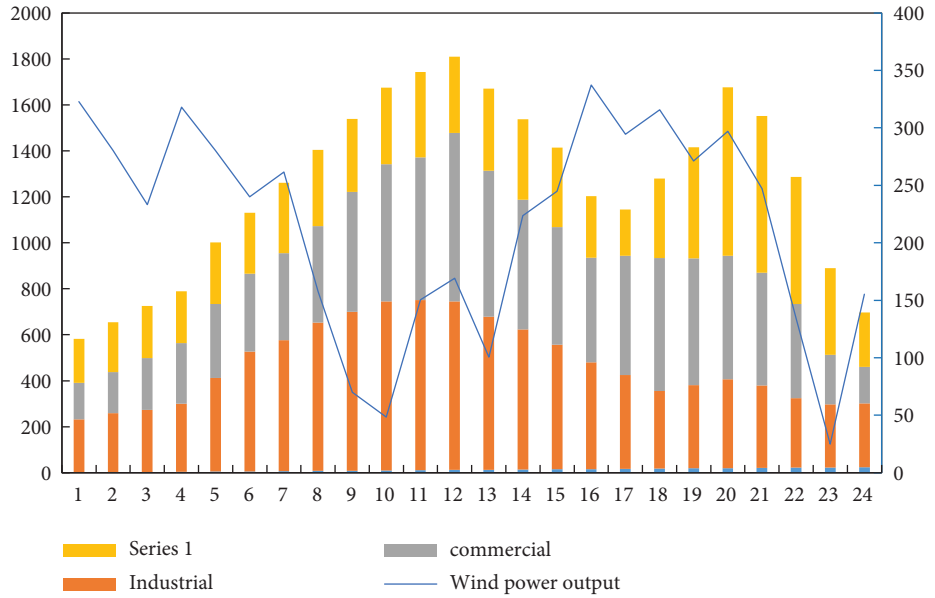

Figure 3: Prediction curves of classified user loads and wind power outputs.

Table 2: TOU correlation coefficients of classified users.

Type of users	Time period			Before TOU	Fluctuation in price	After TOU			Self-elasticity	Cross-elasticity		
	Peak	Flat	Valley			Peak	Flat	Valley		P-F	P-V	F-V
Industrial users	7–14	5–6, 15–21	1–4, 22–24	0.64	Up 53%, down 41%	0.98	0.64	0.30	−0.38	0.03	0.03	0.03
Commercial users	10–14, 18–20	7–9, 15–17, 21-22	1–6, 23–24	0.8	Up 53%, down 41%	1.22	0.8	0.38	−0.12	0.02	0.02	0.02
Residential users	13–14, 19–23	7–12, 15-16, 18	1–6, 17, 24	0.55	Up 50%, down 50%	0.84	0.55	0.26	−0.2	0.02	0.04	0.02

Table 3: Life loss rate of a coal-fired power unit under different variable load amplitudes.

Variable load amplitude	5%	15%	20%	30%	45%	50%	55%	60%	65%	70%	75%	80%
Life loss rate (10^{-4})	0.02	0.04	0.05	0.06	0.08	0.1	0.13	0.16	0.17	0.19	0.2	0.24

power output, and the lowest WE utilization rate is 27.44%. The outcome is closely related to the first-stage model's target function and the antipeaking properties of wind power itself. Furthermore, the largest peak-to-valley difference of the net load curve before optimization is only 720.67 MW, but after optimization, it is 1370.46 MW (without including the TOU, ESS, and WE use). This demonstrates that the proposed scheduling method significantly reduces load variance and peak control costs.

The charging power, discharging power, and SOC of the ESS for each period are illustrated in Figure 6, showing that the SOC of the ESS always remains within the limiting range. The ESS has a peak-shaving power of 467.95 MW. As wind power outputs are low at the six load peak hours of 10 : 00,

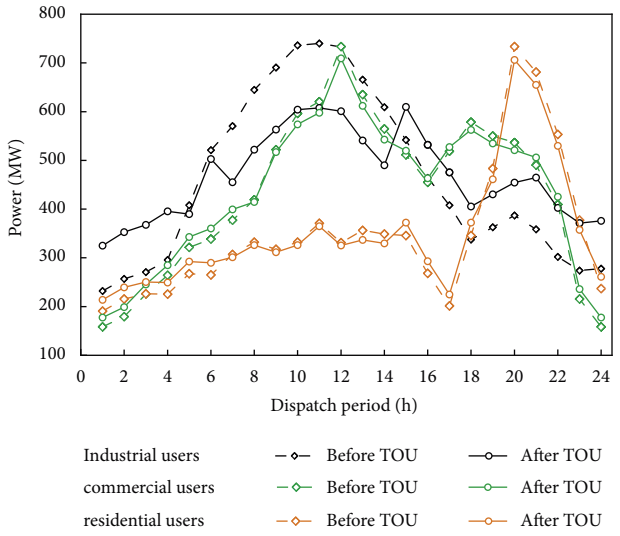

Figure 4: Load curves of industrial, commercial, and residential users before and after TOU.

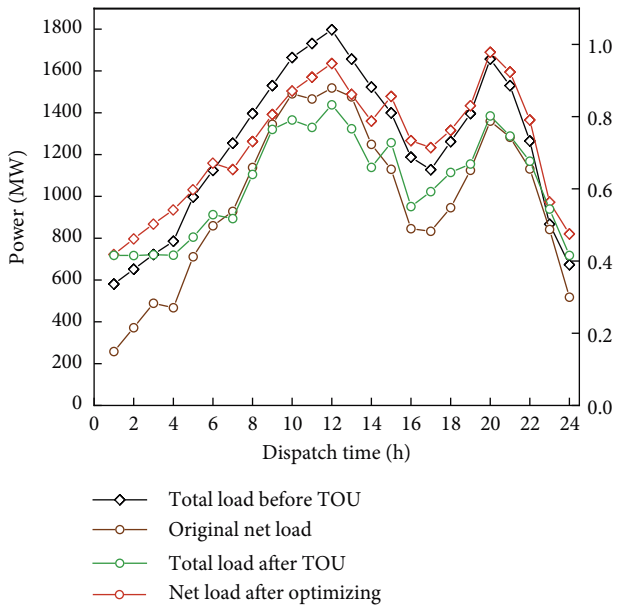

Figure 5: First-stage model optimization results.

11 : 00, 12 : 00, 13 : 00, 21 : 00, and 22 : 00, the ESS is discharged to share peak-shaving pressure with the coal-fired power units at these times. The power of the ESS at valley-filling is 577.71 MW. During the seven load peak hours of 1 : 00, 2 : 00, 3 : 00, 5 : 00, 17 : 00, 18 : 00, and 24 : 00, the ESS is charged to absorb the excess energy generated by the coal-fired power units, reducing the frequency with which coal-fired power units enter DPR and DPRO.

The outputs of the TPUs after optimization at each time period are depicted in Figure 7. The outputs of the three smaller TPUs, units 4, 5, and 6, remain relatively stable during the scheduling period. Units 4 and 6 work in RPR and simply produce the associated coal consumption costs. Consequently, unit 5 runs most often in DPR. Due to their enormous capacities, units 1, 2, and 3 handle the majority of

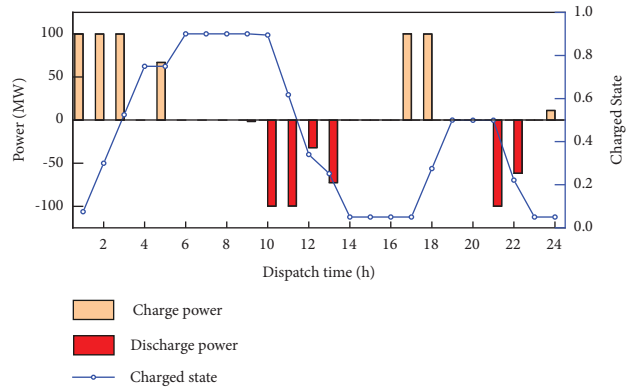

Figure 6: The ESS's SOC, charging power, and discharging power.

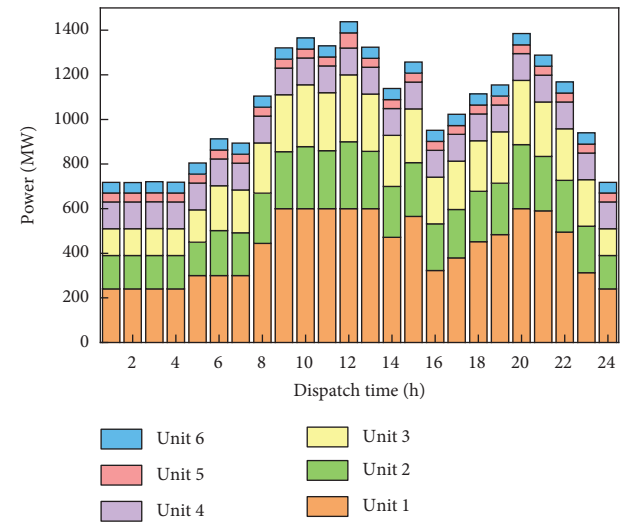

Figure 7: Coal-fired power units' optimal output for each time period.

the peak-shaving work. As the net load curve's fluctuation range has been greatly reduced and the units' peak-shaving efficiency has been strengthened, it is notable that none of the thermal units need to enter DPRO.

3.2.3. Comparative Analysis of Different Scenarios. Four scenarios are established to verify the validity of the proposed model.

Scenario 1: Considering TOU, ESS, and WE utilization. (The model proposed in this study.)

Scenario 2: Considering ESS and WE utilization.

Scenario 3: Considering TOU and ESS, while the wind power is fully integrated into the grid for consumption.

Scenario 4: Considering TOU and WE utilization.

The load characteristic curves and wind power output forecast curves applied in this research serve as the basis for all four scenarios, and the first and second stages of model optimization have the same purposes as before. Figure 8 displays the net load curve optimization outcomes for each scenario. Figure 9 displays the precise output of each TPU per time period in scenarios 2, 3, and 4. All three peak-

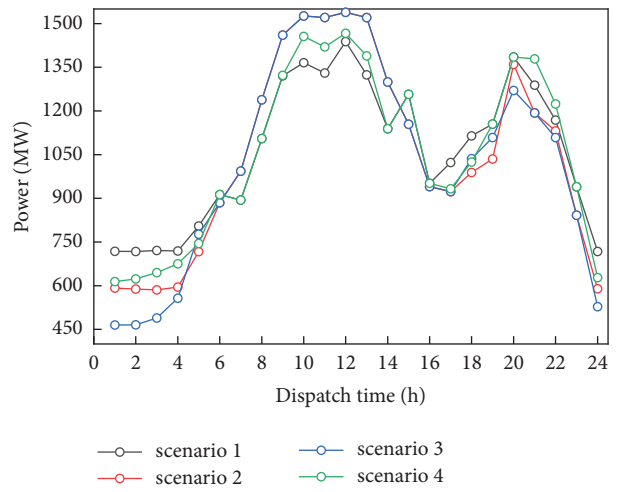

Figure 8: Net load curve of each scenario.

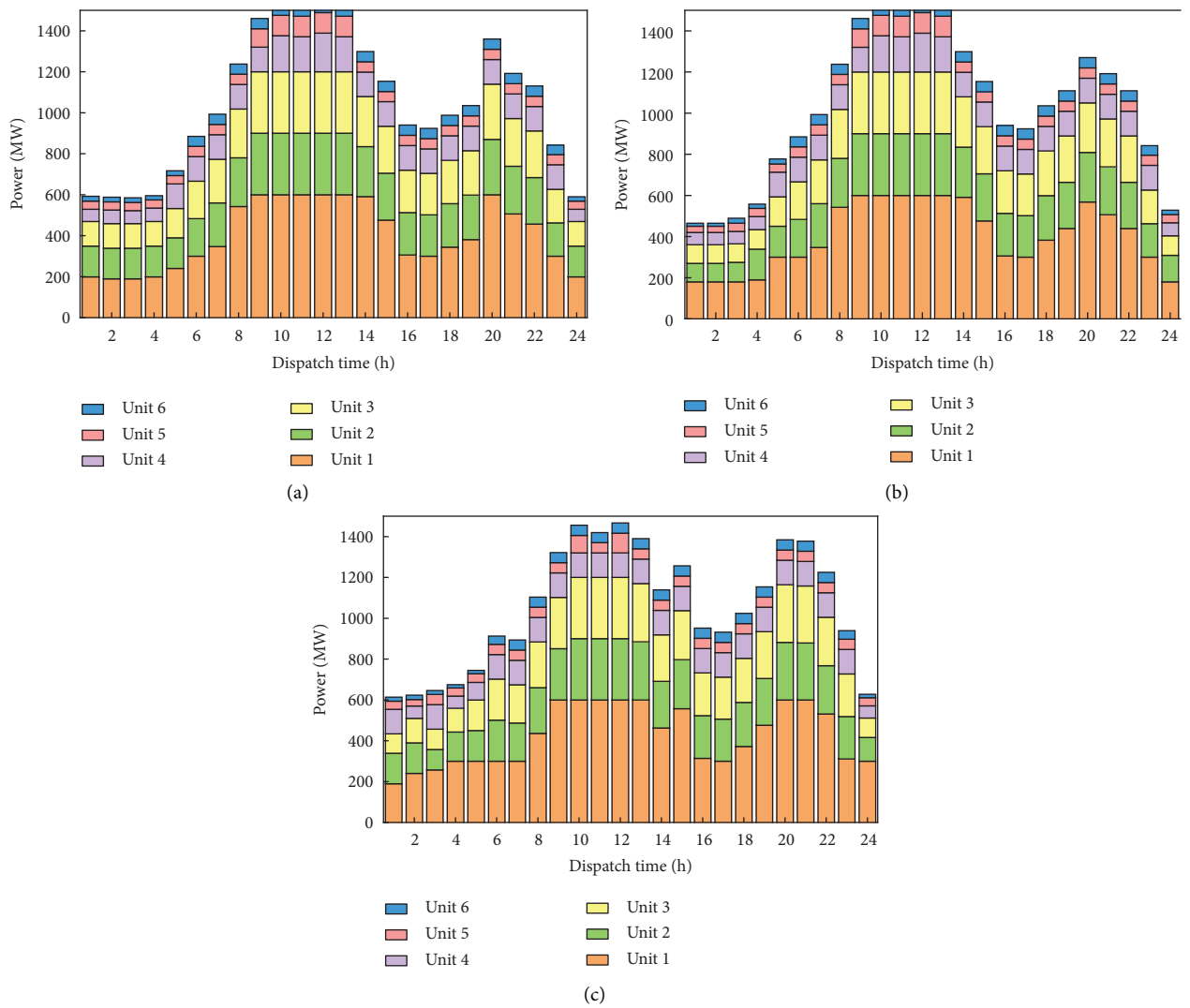

Figure 9: Optimal outputs of thermal power units in each period in scenarios 2, 3, and 4.

Table 4: Comparison of the system peak-shaving cost results in various scenarios.

Scenarios	Total cost	Wind power cost	ESS cost	Carbon cost	Coal cost	Loss of life cost	Oil cost
1	402.53	21.62	15.81	53.83	304.26	7.01	0
2	465.5	21.62	20.43	75.17	303.72	15.14	29.42
3	529.32	15.53	21.04	74.55	300.11	53.36	64.73
4	468.47	21.62	0	73.88	301.59	24.30	47.08

shaving measures (WE utilization rate, TOU, and ESSs) have demonstrable smoothing impacts on the volatility of the net load curve, which can facilitate the consistent adjustment of TPUs' output. The peak-to-valley difference of the net load can be reduced from 1 073.55 MW to 720.67 MW in the TOU environment combined with the ESS if the WE utilization rate is factored into the equation (scenario 1). This markedly lowers the burden of peak regulation and assures the electricity grid's reliable and safe functioning.

With a unit of cost of 10,000 CNY, the calculated system costs under various scenarios are displayed in Table 4. Scenario 1 has the lowest peak-shaving cost (4.0253 million CNY). Scenarios 2, 3, and 4 have peak-shaving costs that are 0.629 million, 1.2679 million, and 0.6594 million CNY higher than that of scenario 1, respectively. These findings demonstrate that coordinated ESS usage and accounting for the rate of WE usage in the TOU environment can significantly improve the economics of peak-shaving in the power system. The prices of coal consumption are similar in all scenarios, and the large calculated decrease of the peak-to-valley difference in the grid's net load caused by optimizing the grid-connected power of WE at all times is the main contributor to the lower costs of the power system. This reduces the net load peak-to-valley difference as well as the frequency with which TPUs enter DPRO, significantly cutting the cost of oil investment and the cost of TPU life loss. This implies that, in contrast to the operational effects of scenarios 1 and 3, the peak output of wind power should be rationalized to ensure the secure and reliable operation of the power system. Specifically, WE utilization should be planned on the basis of the need for low-carbon, economical wind power consumption.

4. Conclusion

The main contributions of this study include the following:

(1) It is verified that rational wind power curtailment can effectively improve the overall economy of the power system, and new evidence for the economical uptake of WE is presented.

(2) A mathematical model for solving the optimal grid-connected wind power throughout the day is constructed. Compared with previous models, it has greater significance for practical guidance on realizing the economical consumption of WE. Simulated data vividly illustrate the favorable effect of rational energy curtailment on the thermal power peaking cost and grid net load fluctuation.

(3) The results of the operational simulations show that the peak-shaving cost of the strategy devised in this study is 4,025,300 CNY. Compared with the scheduling model in which wind power is completely integrated into the grid, the overall costs are decreased by 1,267,900 CNY, the costs of carbon are decreased by 207,200 CNY, and the costs of DPR for TPUs are decreased by 1,100,800 CNY. The overall peak-shaving cost of the system can be reduced by up to 23.95%, and the TP DPR cost can be reduced by up to 90.06%.

To further explore the economical consumption of WE and improve the safety and economy of the operation of new power systems, future research could focus on the following:

(1) Incorporation of the wind power output forecast error, which is not studied in this study. This would enhance the practical significance of the proposed method.

(2) Consideration of the influence of the capacity configuration of the ESS or other attributes on the participation of wind power in optimal dispatch, as the capacity of the ESS in this study is a fixed value

Data Availability

All data, models, and code generated or used during the study are included within the article.

Conflicts of Interest

The authors declare that they have no conflicts of interest.

References

[1] D. M. Newbery, "Towards a green energy economy? The EU Energy Union's transition to a low-carbon zero subsidy electricity system – lessons from the UK's Electricity Market Reform," *Applied Energy*, vol. 179, pp. 1321–1330, 2016.

[2] L. Zhang, J. Kuang, B. Sun, F. Li, and C. Zhang, "A two-stage operation optimization method of integrated energy systems with demand response and energy storage," *Energy*, vol. 208, Article ID 118423, 2020.

[3] J. Lee and A. Bath, "Global Wind Report 2022," https://gwec.net/, "[online]," 2020.

[4] X. Zhang, C. Ma, X. Song, Y. Zhou, and W. Chen, "The impacts of wind technology advancement on future global energy," *Applied Energy*, vol. 184, pp. 1033–1037, 2016.

[5] R. Zhang, T. Jiang, L. Bai et al., "Adjustable robust power dispatch with combined wind-storage system and carbon capture power plants under low-carbon economy,"

International Journal of Electrical Power & Energy Systems, vol. 113, pp. 772–781, 2019.

[6] M. Hedayati-Mehdiabadi, K. W. Hedman, and J. Zhang, "Reserve policy optimization for scheduling wind energy and reserve," *IEEE Transactions on Power Systems*, vol. 33, no. 1, pp. 19–31, 2018.

[7] K. Grimsrud, C. Hagem, A. Lind, and H. Lindhjem, "Efficient spatial distribution of wind power plants given environmental externalities due to turbines and grids," *Energy Economics*, vol. 102, Article ID 105487, 2021.

[8] J. Cullen, "Measuring the environmental benefits of wind-generated electricity," *American Economic Journal: Economic Policy*, vol. 5, no. 4, pp. 107–133, 2013.

[9] Y. Yasuda, L. Bird, E. M. Carlini et al., "C-E (curtailment – energy share) map: an objective and quantitative measure to evaluate wind and solar curtailment," *Renewable and Sustainable Energy Reviews*, vol. 160, Article ID 112212, 2022.

[10] D. Newbery, "National Energy and Climate Plans for the island of Ireland: wind curtailment, interconnectors and storage," *Energy Policy*, vol. 158, Article ID 112513, 2021.

[11] M. Baudry and C. Bonnet, "Demand-pull instruments and the development of wind power in europe: a counterfactual analysis," *Environmental and Resource Economics*, vol. 73, no. 2, pp. 385–429, 2019.

[12] F. Ugranli, E. Karatepe, and A. H. Nielsen, "MILP approach for bilevel transmission and reactive power planning considering wind curtailment," *IEEE Transactions on Power Systems*, vol. 32, no. 1, pp. 652–661, 2017.

[13] D. Argüeso and S. Businger, "Wind power characteristics of Oahu Hawaii," *Renewable Energy*, vol. 128, pp. 324–336, 2018.

[14] P. Scarabaggio, S. Grammatico, R. Carli, and M. Dotoli, "Distributed demand side management with stochastic wind power forecasting," *IEEE Transactions on Control Systems Technology*, vol. 30, no. 1, pp. 97–112, 2022.

[15] A. Marot, A. Kelly, M. Naglic et al., "Perspectives on future power system control centers for energy transition," *Journal of Modern Power Systems and Clean Energy*, vol. 10, no. 2, pp. 328–344, 2022.

[16] G. C. van Kooten, "The economics of wind power," *Annual Review of Resource Economics*, vol. 8, no. 1, pp. 181–205, 2016.

[17] V. Ongoma, "Socio-economic and environmental analysis of wind power projects as viable renewable energy resources in Kenya," *African Journal of Science, Technology, Innovation and Development*, vol. 10, no. 5, pp. 525–538, 2018.

[18] A. Turk, Q. Wu, M. Zhang, and J. Østergaard, "Day-ahead stochastic scheduling of integrated multi-energy system for flexibility synergy and uncertainty balancing," *Energy*, vol. 196, Article ID 117130, 2020.

[19] L. Bird, D. Lew, M. Milligan et al., "Wind and solar energy curtailment: a review of international experience," *Renewable and Sustainable Energy Reviews*, vol. 65, pp. 577–586, 2016.

[20] F. Xu, Y. Wang, and J. Yang, "Generation scheduling model and application for wind-thermal power system considering security constraints," *Automation of Electric Power Systems*, vol. 38, no. 21, pp. 114–120, 2014.

[21] Y. H. Wang, N. Li, B. Yuan, F. Q. Zhang, and J. S. Feng, "Discussion on the rReasonable curtailment problems in highly renewable power system planning," *Electric Power*, vol. 50, no. 11, pp. 8–14, 2017.

[22] Y. B. Wang, G. Cai, C. Zheng, D. Y. Yang, Z. L. Sun, and Y. Fang, "Study on the accommodation approach of wind power based on rational wind power casting," *Electrical Measurement & Instrumentation*, vol. 53, no. 11, pp. 45–50, 2016.

[23] R. Golden and B. Paulos, "Curtailment of renewable energy in California and beyond," *The Electricity Journal*, vol. 28, no. 6, pp. 36–50, 2015.

[24] X. Liu, S. Liu, S. T. Yu, T. Sun, and H. Y. Guo, "Design of Peak Load Regulation Capacity Compensation Mechanism for New Power System Flexibility Enhancement," *Power System Technology*, pp. 1–10, 2022.

[25] L. Ma, Z. Wang, Z. Lu, X. Lu, and F. Wan, "Integrated strategy of the output planning and economic operation of the combined system of wind turbines-pumped-storage-thermal power units," *IEEE Access*, vol. 7, pp. 20567–20576, 2019.

[26] Y. Li, B. Wang, Z. Yang, J. Li, and G. Li, "Optimal scheduling of integrated demand response-enabled community-integrated energy systems in uncertain environments," *IEEE Transactions on Industry Applications*, vol. 58, no. 2, pp. 2640–2651, 2022.

[27] N. Mahdavi and J. H. Braslavsky, "Modelling and control of ensembles of variable-speed air conditioning loads for demand response," *IEEE Transactions on Smart Grid*, vol. 11, no. 5, pp. 4249–4260, 2020.

[28] O. Alrumayh and K. Bhattacharya, "Flexibility of residential loads for demand response provisions in smart grid," *IEEE Transactions on Smart Grid*, vol. 10, no. 6, pp. 6284–6297, 2019.

[29] Z. Li, Y. Xu, X. Feng, and Q. Wu, "Optimal stochastic deployment of heterogeneous energy storage in a residential multienergy microgrid with demand-side management," *IEEE Transactions on Industrial Informatics*, vol. 17, no. 2, pp. 991–1004, 2021.

[30] A. Tomczewski and L. Kasprzyk, "Optimisation of the structure of a wind farm—kinetic energy storage for improving the reliability of electricity supplies," *Applied Sciences*, vol. 8, no. 9, p. 1439, 2018.

[31] L. Zhang, J. Zhang, X. H. Jian, F. Zhang, and X. S. Han, "Unit commitment with energy storage considering operation flexibility at sub-hourly time scales," *Automation of Electric Power Systems*, vol. 42, no. 16, pp. 48–56, 2018.

[32] H. Hamidpour, J. Aghaei, S. Pirouzi et al., "Coordinated expansion planning problem considering wind farms, energy storage systems and demand response," *Energy*, vol. 239, Article ID 122321, 2022.

[33] M. Hosseini Imani, P. Niknejad, and M. R. Barzegaran, "Implementing Time-of-Use Demand Response Program in microgrid considering energy storage unit participation and different capacities of installed wind power," *Electric Power Systems Research*, vol. 175, Article ID 105916, 2019.

[34] M. MohammadGholiha, K. Afshar, and N. Bigdeli, "Optimal reserve determination considering demand response in the presence of high wind penetration and energy storage systems," *Iranian Journal of Science and Technology, Transactions of Electrical Engineering*, vol. 44, no. 4, pp. 1403–1428, 2020.

[35] H. Bitaraf and S. Rahman, "Reducing curtailed wind energy through energy storage and demand response," *IEEE Transactions on Sustainable Energy*, vol. 9, no. 1, pp. 228–236, 2018.

[36] A. Jamali, J. Aghaei, M. Esmaili et al., "Self-scheduling approach to coordinating wind power producers with energy storage and demand response," *IEEE Transactions on Sustainable Energy*, vol. 11, no. 3, pp. 1210–1219, 2020.

[37] Y. Li, J. Wang, D. Zhao, G. Li, and C. Chen, "A two-stage approach for combined heat and power economic emission dispatch: combining multi-objective optimization with integrated decision making," *Energy*, vol. 162, pp. 237–254, 2018.

[38] B. Miao, J. Lin, H. Li et al., "Day-ahead energy trading strategy of regional integrated energy system considering energy cascade utilization," *IEEE Access*, vol. 8, pp. 138021–138035, 2020.

[39] Z. Li, Y. Xu, S. Fang, Y. Wang, and X. Zheng, "Multiobjective coordinated energy dispatch and voyage scheduling for a multienergy ship microgrid," *IEEE Transactions on Industry Applications*, vol. 56, no. 2, pp. 989–999, 2020.